New Astronomy 27 (2014) 1–12

Contents lists available at ScienceDirect

New Astronomy

journal homepage: www.elsevier.com/locate/newast

APASS BVgri search for and characterization of RR Lyr variables candidate members of the Aquarius halo stream

Ulisse Munari [a,*], Arne Henden [b], A. Frigo [c]

[a] INAF Astronomical Observatory of Padova, 36012 Asiago (VI), Italy
[b] AAVSO, 49 Bay State Road, Cambridge, MA 02138, USA
[c] ANS Collaboration, Astronomical Observatory, 36012 Asiago (VI), Italy

HIGHLIGHTS

- We obtained BVgri photometry of 100,000 stars over the Aquarius stream sky area.
- 15 separate observing epochs were used in looking for RR Lyr variables.
- 71 RR Lyr variables were discovered providing a census complete to V = 15.2 or 8 kpc.
- Pulsation periods, temperatures, lightcurves, magnitudes and distances are given.

ARTICLE INFO

Article history:
Received 6 June 2013
Received in revised form 5 July 2013
Accepted 20 July 2013
Available online 9 August 2013

Communicated by P.S. Conti

Keywords:
Stars
Variables
RR Lyr – surveys – galaxy
Structure

ABSTRACT

The Aquarius stream has been recently discovered in the course of the RAVE Survey. It is a chemically coherent structure, originating from the tidal disruption of a 12 Gyr, [Fe/H] = −1.0 globular cluster. We have surveyed a ~ 284 deg^2 area of the sky containing the 15 known members of the Aquarius stream looking for RR Lyr variables. RR Lyr variables are primary distance indicators and discovering some of them firmly associated with the Aquarius stream would provide a 3D representation of its Galactic orbit and would probe the spatial structure of the Galactic gravitational potential. During September and October 2012, we have obtained on-purpose, epoch photometry in the Landolt B, V and Sloan g, r, i bands with the APASS South telescopes located at Cerro Tololo. Our data are uniformly complete to $V = 15.2$ mag over the whole surveyed area, the faintest recorded stars reaching $V = 18$ mag. We have found 71 RR Lyr variables, and a firm pulsation period was derived for 53 of them. Our census of RR Lyr variables is complete to a distance of 8 kpc from the Sun. For all objects we provide distances and light- and color-curves, mean values and amplitudes in all five *BVgri* passbands, finding charts and accurate local photometric sequences. About half of the RR Lyr variables we have discovered were previously known, but we provide the first multi-band photometric data. They were in fact mostly discovered as by-products of white-light patrol searches for optical counterparts to gamma-ray bursters or potentially hazardous asteroids.

1. Introduction

Relics of the hierarchical process of Milky Way formation are present as spatial and kinematic substructures of the Halo. Closer to the Sun, the spatial coherence of streams is increasingly difficult to discern against field stars and they are best visible as velocity coherent structures. The Aquarius stream was discovered by Williams et al. (2011, hereafter W + 11) in the RAVE data (RAdial Velocity Experiment; Steinmetz et al., 2006; Zwitter et al., 2008; Siebert et al., 2011), as 15 outliers in the spatial arrangement of the velocity distribution of RAVE stars, which are located in the Aquarius constellation and appear to move almost directly toward us at −200 km/s. We confirmed with unpublished Asiago Echelle high resolution observations their radial velocities, that place them completely aside from field stars in the same region of the sky. Wylie-de Boer et al. (2012, hereafter W + 12) presented an abundance analysis of six of the Aquarius stars from high resolution spectra. Their mean metallicity is [Fe/H] = −1.0 with a dispersion of just 0.1 dex, indicating that they are a chemical coherent structure and therefore not the result of dynamical resonances. The abundances of Ni, Na, O, Mg and Al exclude that the Aquarius stream may have originated from the disruption of a dwarf galaxy. They instead indicate a 12 Gyr old, [Fe/H] = −1.0, [Fe/α]-enhanced globular cluster as the origin of the Aquarius stream.

According to W + 12, the stream appears to be plunging in toward the solar neighborhood from the south and is likely to extend out to the north on the opposite side of the Galactic disk. As the

* Corresponding author. Tel.: +39 (0)424 600033; fax: +39 (0)424 600023.
E-mail address: ulisse.munari@oapd.inaf.it (U. Munari).

1384-1076/$ - see front matter © 2013 Elsevier B.V. All rights reserved.
http://dx.doi.org/10.1016/j.newast.2013.07.007

stream members fall toward the disk of the Galaxy, their velocity increases. The measured values range from −160 km/s for the most distant known members, located at about 3 kpc, to −210 km/s for those at 1 kpc. The distance to known members is however only crudely estimated from fitting the atmospheric parameters to isochrones. Knowing robust distances to many more members would enable the reconstruction of the 3D shape of the Galactic orbit followed by the Aquarius stream, and this could be used to trace and measure the Galactic gravitational potential in the solar suburb. It would also be important to probe longer distances than the 3 kpc allowed by RAVE observations, where the stream should be arching away from the direction from which the closest members appear to come. We therefore need to search for member stars which are intrinsically bright, easily distinguishable from the vastly more abundant field stars and able to provide accurate individual distances. They are the RR Lyr variables, which are abundant in globular clusters, easy to spot thanks to their large and characteristic photometric variability, and for which their absolute magnitude is well known.

RR Lyrae variables (hereafter RRvar) are relatively low mass stars (∼0.7–0.8 $M_\odot$), lying on the horizontal branch defined by stars undergoing core helium burning (Kolenberg, 2012; Smith, 2012). They are old, metal poor stars, first identified in globular clusters, for which they were initially named *cluster variables*. They pulsate with large amplitudes (up to about one magnitude in *V*) and short periods (from 0.2 to 1.0 days, with a maximum frequency around 0.50–0.55 days). Bailey (1902) divided RRvar into three subclasses (a, b, c) based upon their periods and light curve shapes. Modern classification uses two types only: RRab and RRc. Stars of the RRab variety are pulsating in the fundamental radial mode, while those of the RRc type pulsate in the first overtone radial mode. Some RRvar are known to simultaneously pulsate in both modes. Since the seminal work of Shapley (1918) that showed how all RRvar within a given cluster share the same apparent magnitude, it was realized that their absolute magnitude shows little dispersion and therefore RRvar were standard candles of high potential.

This paper reports the results of our extensive search for and characterization of RRvar that are candidate members of the Aquarius halo stream. Our list of RRvar candidates is intended to be the starting point for highly focused, follow-up spectroscopic observations that will measure radial velocity and chemical abundances of the candidates to segregate stream members from field objects. A number of RRvar are already known or suspected over the area of the sky covered by the Aquarius stream (hereafter AqS area).

The ROTSE-I telescope was located in Los Alamos (New Mexico), and was composed of four small telescopes (actually Canon FD 200 mm f/1.8 telephoto lenses feeding light to four 2048×2048 CCDs) mounted on a rapidly slewing platform. It was originally designed to find the optical counterparts to gamma-ray bursters. While waiting for a trigger from a gamma-ray burster, the telescope was used in a patrol mode, which scanned the sky. The observations were obtained in unfiltered mode (white light). Kinemuchi et al. (2006, hereafter K + 06) analyzed the ROTSE-I data and published mean magnitude, amplitude and pulsation period for 1188 RRvar, 14 of them residing within the AqS area. Working on the same set of ROTSE-I data, Hoffman and McNamara (2009, hereafter H + 09) identified additional variables, 8 of them in the AqS area.

The Lowell Observatory Near Earth Object Survey (LONEOS) had as its primary goal the detection of potentially hazardous asteroids. Situated on the Anderson Mesa outside Flagstaff, Arizona, LONEOS was carried out with a 0.6 m Schmidt telescope equipped with a 2048 × 4096 CCD, operated in unfiltered mode (white light). The proximity of AqS area to the ecliptic means that it was visited many times by LONEOS. Miceli et al. (2008, hereafter M + 08) investigated the LONEOS database and identified 838 RRvar, 48 of them residing within the AqS area (many of them in common with ROTSE-I), and published mean magnitudes, amplitudes and pulsation periods for them.

Sesar et al. (2010) looked for RRvar in the Sloan SDSS survey data. There is a small overlap of their data with the AqS area, containing 9 of their RRvar, all of them very faint objects (down to $V = 20$ mag).

An additional RRvar within the AqS area was found by Keller et al. (2008) who identified it among the archived observations of the Southern Edgeworth–Kuiper Belt Object (SEKBO), a multi-epoch, two-color imaging survey of a 10° band centered on the ecliptic. Observations were obtained with the Mount Stromlo Observatory 1.27 m Great Melbourne Telescope that was previously used for the MACHO microlensing survey.

Two more RRvar within the AqS area are listed among the 1500 variables discovered by Henden and Stone (1998) with the US Naval Observatory 20 cm Flagstaff Astrometric Scanning Transit Telescope (FASTT) while they used it to obtain astrometric information in 16 equatorial fields in support of the Sloan Digital Sky Survey.

Finally, a few more RRvar within the AqS area are listed in the 2013 on-line version of the General Catalog of Variable Stars (GCVS[1]).

2. Goals

Given the great relevance of RRvar to define the 3D structure of the Aquarius stream, its Galactic orbit and the possibility to probe the Galactic gravitational potential, we have undertaken the present study motivated by the following arguments.

The distribution on the sky of previously known RRvar over the AqS area is markedly patchy. Does this reflect a truly dis-homogeneous distribution, with obvious consequences on the inferred 3D distribution of the Aquarius stream, or is it just the result of observational biases, like uneven sky coverage by previous patrol programs? To answer these questions, we monitored a large area of the sky whose boundaries include all the previously known stream members (a total of 284 deg^2, cf. Fig. 1), and evenly observed all its parts.

The vast majority of RRvar previously known over the AqS area of the sky are by-products of white-light patrol searches for optical counterparts to gamma-ray bursters, or white-light searches of potentially hazardous asteroids. As such, they lack multi-band photometric information, and the quoted *V*-band magnitudes and amplitudes are estimated from unfiltered observations. Given the accuracy reached by available calibrations of the absolute magnitude of RRvar, a true *V*-band characterization flanked by multi-band photometric information is clearly welcome.

Gathering accurate and simultaneous multi-band color-light-curves of RRvar enables the derivation of the surface effective temperature ($T_{\rm eff}$) and its variation along the pulsation cycle, a useful prior to atmospheric analysis from high-resolution, high S/N spectra. Such spectra are essential to prove the membership of the candidate RRvar in the Aquarius stream, not only in terms of barycentric radial velocities, but also in terms of chemical abundances, given the well defined chemical homogeneity of known members of the Aquarius stream (cf. W + 12).

The distribution in magnitude of RRvar previously known over the AqS area is different from that of field stars. Its slope is flatter, indicating that the fraction of missed RRvar increases with fainter magnitudes, and therefore with increasing distance from the Sun. Possible solutions for the Galactic orbit of AqS suggest that its orbit could be arching to a distance of about 5 kpc along the line of sight

[1] on-line at http://www.sai.msu.su/groups/cluster/gcvs/gcvs/.

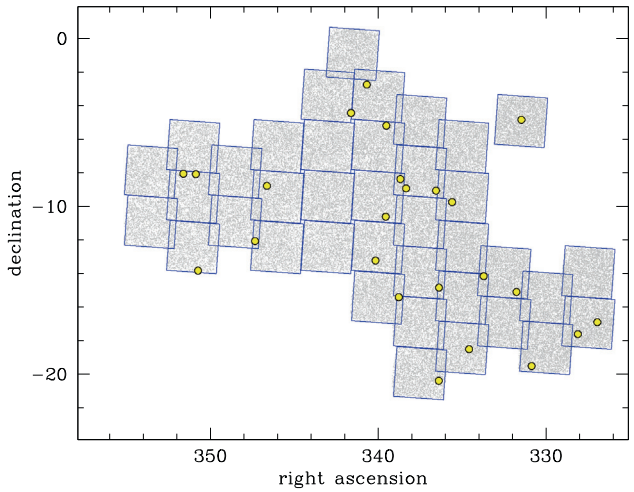

Fig. 1. The area surveyed for RR Lyr variables. The 92,876 stars with simultaneous measurements in all five B,V,g,r,i APASS bands on at least 8 different observing epochs (8-epochs sample) are plotted in the background. The squares outline the 38 monitored fields. The dots mark the known Aquarius members from Williams et al. (2011) discovery paper plus a few additional members later identified (M. Williams private communication).

(K. Freeman, private communication). An RRvar, at the high galactic latitude of the Aquarius line of sight, would have a brightness of $V\sim$14.2 mag at 5 kpc (for E_{B-V} = 0.056 reddening, [Fe/H] = −1.0 metallicity by W + 12, and adopting the calibration of RRvar absolute magnitude by Benedict et al. (2011). To be on the safe side, we have planned our observations to provide a complete census of all RRvar present in the surveyed area down to $V\sim$15.0/15.2 mag, corresponding to a distance of 8 kpc.

The classification as RRvar of variables previously discovered by white light patrol searches over the AqS area of the sky was done in an automated way and without the support of multi-band photometric data. All types of pulsating stars display tight brightness-color correlations that greatly help to distinguish true pulsators from impostors. Furthermore, searching for coherent pulsation periods simultaneously present in data obtained in different photometric bands provides more reliable results than those obtained in just white light (plagued by a lower number of points and larger dependence of the effective wavelength on airmass and sky conditions). Thus wrong classification and/or wrong pulsation periods could affect previously reported RRvar in AqS, and a check would be worthwhile. Indeed, we discovered a few cases of wrong pulsation periods as well as wrong classifications, as it will be outlined in following sections.

3. Observations

The large area on the sky covered by the Aquarius stream requires instruments with a very large field of view. We selected to obtain multi-band photometry from CTIO (Chile) with the same equipment used for the APASS all sky photometric survey, separately from the main Survey program (Henden, 2013). A pair of twin remotely controlled, small telescopes obtain simultaneous CCD observations over five optical bands: B,V (tied to the equatorial standards of Landolt, 2009) and g,r,i bands (tied to the 158 primary standards given by Smith et al., 2002Please note that the reference Smith et al. 2002, Castelli and Kurucz (2004), and Landolt 2009 is cited but not provided in the reference list. check and provide., that define the Sloan "prime" photometric system; all mentions of g,r,i in this paper refer to g', r', i' variant). The telescopes are 20 cm f/3.6 astrographs feeding Apogee U16m cameras (4096 × 4096 array, 9 μm pixels), that cover a field 2.9 deg wide with a 2.6 arcsec/pix plate scale. One telescope exposes the B and g bands, while the other in parallel exposes the V, r and i bands. The photometric filters are of the dielectric multi-layer type and are produced by Astrodon. Transmission curves and photometric performances of Astrodon filters are discussed and compared with more conventional types of photometric filters in Munari et al. (2012) and Munari and Moretti (2012).

The observations for this paper were obtained with fixed exposure times (different and optimized for each photometric band), set to detect V = 17 stars at S/N = 5 on a single exposure. Stars brighter that V = 10 may saturate under optimal seeing conditions. Differential photometry within a given field is accurate to better than 0.010 mag. Absolute photometric calibration is obtained against the APASS main survey data. An evaluation of the high accuracy of APASS photometric and astrometric products has been presented by Munari et al. (2013b) for the half-million stars spectroscopically observed by the RAVE survey, and further tests and comparisons are carried out by Henden (2013). The sparsely populated stellar field in Aquarius means that aperture photometry is fully adequate to measure stellar magnitudes, without the need to revert to PSF fitting.

The area to be surveyed, was divided into 38 pointings, highlighted in Fig. 1, with different degree of overlap between adjacent pointings, to both reflect the varied density of known stream members and to explore the effect of the number of available observations on the detection of RRvar and characterization of their lightcurves. The 38 pointings were visited on 15 different epochs, separated by at least a couple of hours and grouped up to four visits per night. A total of 246,968 stars were detected in at least one band on one epoch, and 92,876 stars were those detected simultaneously in all five bands on at least 8 different epochs (hereafter termed *8-epochs sample*). As it will be shown in the next section, 8 epochs are usually enough to derive the pulsation period of an RR Lyr with the data here at disposal, as well as to discriminate them from other types of variables on the basis of the amplitude of variation, colors and the tight correlation between brightness and color that they exhibit.

The seeing and sky transparency conditions varied among the 15 observing epochs, so fainter stars were not always detected. Fig. 2 shows how many times the stars were detected (simultaneously on all bands) as function of their magnitude: $V \leqslant 14.0$ mag stars were detected and accurately measured on all 15 observing epochs, while $V \leqslant 15.4$ mag stars were detected and measured on average on 8 observing epochs. The right panel of Fig. 3 shows the distribution in magnitude of the 92,876 stars of the 8-epoch sample. The distribution suggests that the detection is complete for $V \leqslant 15.2$ mag stars.

4. Searching for and characterization of the variable stars

To discover the variables stars among the surveyed sample, we computed the rms of recorded data and plotted it versus the brightness, separately for all bands. The photometric bands providing the sharpest and cleanest distributions were V,g and r. To further increase the sensitivity of variability detection, we elected to average the V,g and r band data. We define *Vrg* magnitudes and colors as

$$Vgr\ \text{mag} = \frac{V + g' + r'}{3} \tag{1}$$

$$Vgr\ \text{color} = \frac{(V - r') + (g' - r')}{2} \tag{2}$$

The 92,876 stars of the 8-epoch sample are plotted in Fig. 4, where the yellow line marks the progression of rms with magnitude. Poissonian noise controls its rise at fainter magnitudes, while saturation is responsible for the upturn at mag ⩽ 10. We consider

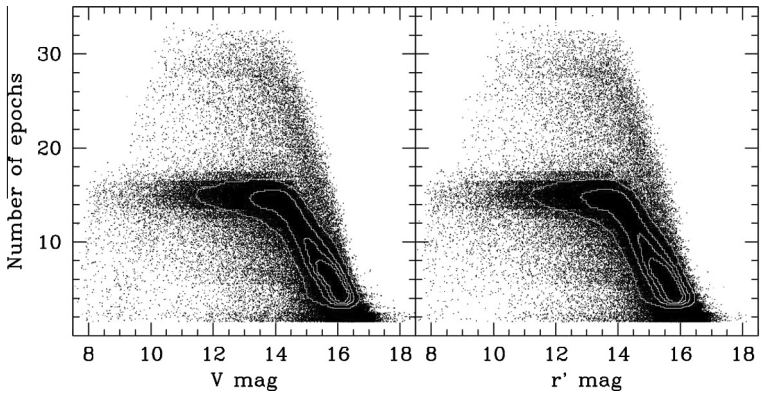

Fig. 2. Number of epochs as function of magnitude for the 202,545 detected stars. To increase visibility, the integer number of epochs is randomly smeared by up to ±0.5. Stars brighter than 14 mag are detected on each of the 15 epochs that were on average exposed on all pointed fields. With increasing faintness, the number of detections begins to decline. The less populated, steeper arm leveling off at 30 epochs is populated by stars in the overlap regions between adjacent fields. Isocontours are drawn at 10%, 30%, 50% and 70% of peak density.

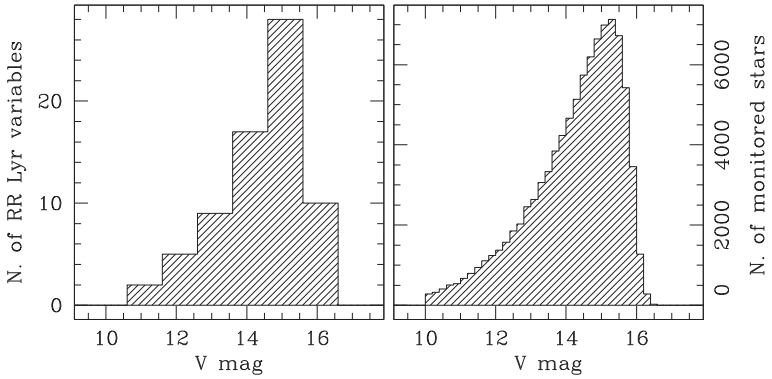

Fig. 3. Distribution in V mag (mean value) of detected RR Lyr variables (1.0 mag steps) compared to that of detected field stars stars (0.2 mag steps, for the 92,876 stars of the 8-epochs sample).

as highly probable variable all the 284 stars fainter than 10 mag and lying above the pink line which marks the 4σ limit in the distribution of Fig. 4, and that do the same in the equivalent plots for V,g and r data treated separately. In this paper we focus only on the RRvar among them, the other type of variables are investigated elsewhere (Munari et al., 2013a).

RRvar span a small range in colors. To isolate the candidate RRvar we re-plotted the same 92,876 stars of Fig. 4 on the color-amplitude diagram of Fig. 5. The average color (from APASS general survey) of RRvar listed in the 2013 on-line version of the GCVS is Vgr = +0.12. Starting from this color, we explored the data in Fig. 5 moving progressively outward in both color directions. We kept expanding the color boundaries until further expansion did not produce any new RRvar. The whole area surveyed is contoured in red in Fig. 5. The stars contained therein, which also lie above the 4σ pink line in Fig. 4, were studied individually. To assess our detection threshold, and to avoid introducing any bias, all of these stars were investigated, *including* those that were already known as a variable. Only when the search for and characterization of all RRvar in the surveyed field was completed did we turn to literature for a comparison (see below). We detected a total of 71 RRvar, and a firm pulsation period was derived for 53 of them.

4.1. Completeness of detection

Fig. 3 compares the distribution in magnitude of the 71 RRvar we discovered with that of the field stars. The two distributions are identical, indicating that the fraction of RRvar present among the surveyed stars does not depend on brightness. The distribution in magnitude of field stars suggests that their detection is complete to $V \leqslant 15.2$, from which we may infer that the discovery of RRvar is also complete to $V \leqslant 15.2$.

4.2. Pulsation periods

Searching for pulsation periods, Fourier analysis was initially attempted, but it was later abandoned given the complexity of the resulting power spectra, dominated by a large number of aliases and interference from the spectral window given the interplay among the small number of observational points, the shortness of the pulsation period and the time extent of the observing interval. Other methods, like phase dispersion minimization, also did not easily converge. A far more reliable, even if much more time consuming method, turned out to be simultaneous eye inspection of light- and color-curves spanning the expected period range. For each star, a movie was created in which the range in period from 0.15 to 1.05 days was explored through about 50,000 frames, equally spaced in the frequency space. Watching the movie, the eye easily spotted the correct pulsation period. This was further inspected and refined on second pass, finer step movies. Exploring the whole 0.15 to 1.05 days range guaranteed the uniqueness of the derived period.

We were able to obtain from eye inspection firm pulsation periods for 53 RRvar discovered within the limits of the red-contoured region of Fig. 5. These 53 RRvar are listed in Table 1. Among them, 35 were previously known in literature, and 18 are brand new

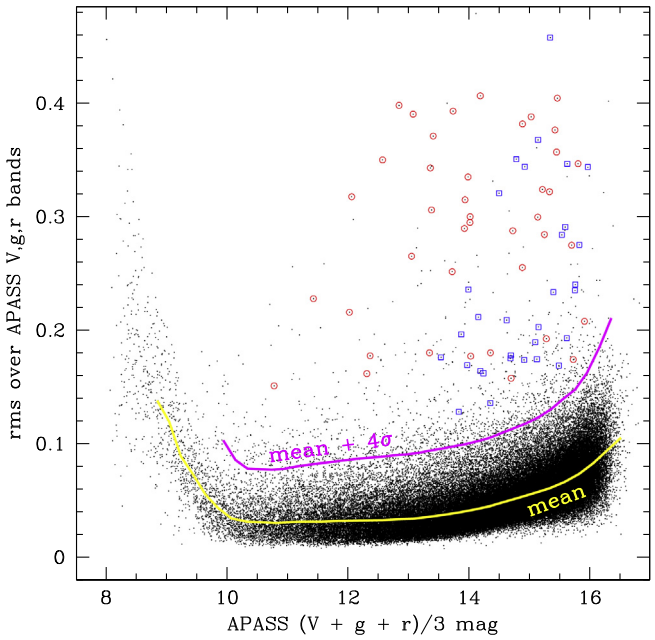

Fig. 4. Position on the magnitude – rms plane for the 92,876 stars of the 8-epochs sample. The magnitudes (and corresponding rms) are computed as averages over the V,g,r bands, which are those returning the data with the highest S/N. The upturn at $\leqslant$10 mag is caused by saturation effects. All the 71 RR Lyr variables discovered in this study are marked; red circles indicate those with a counterpart in literature, those with blue squares are our new discoveries. (For interpretation of the references to colour in this figure caption, the reader is referred to the web version of this article.)

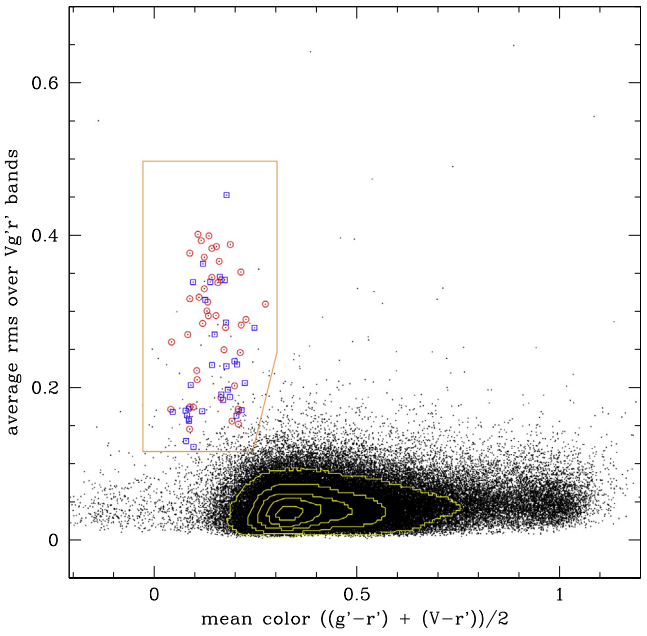

Fig. 5. The same 92,876 stars of Fig. 4 (8-epochs sample) are now plotted on the color – amplitude of variation plane. The red circles mark the RR Lyr variables that we independently re-discovered in this paper and that have a counterpart in literature, while the blue squares mark the brand new ones. (For interpretation of the references to colour in this figure caption, the reader is referred to the web version of this article.)

products of the present study. Fig. 6 presents as an example the light- and color-curves for two of them, one for each of the RRab and RRc types. The whole set of light- and color-curves for the 53 RRvar in presented in Figs. S14–S18 (available electronic only[2]). Among the 35 RRvar in Table 1 which were previously known, we corrected three wrong classifications and three pulsation periods, as outlined in the individual notes below. On all other cases, our independent determination of the pulsation period turned out to be identical to that of literature within the combined uncertainties (about 0.0001 day).

APASS J330.4746–05.4981. K + 06 lists P = 0^d.42822 for this star, while we found instead P = 0^d.2995. The two light- and color-curves are compared in Fig. 7. Our data, while marginally compatible with P = 0^d.42822, provide a better and sharper appearance when plotted against the P = 0^d.2995 period. RRvar of periods in the neighborhood of P = 0^d.42822 usually display amplitudes double the observed ΔV= 0.48, which instead would be the expected value for a P = 0^d.2995 period (cf. Fig. 12). On the other hand, a P = 0^d.2995 would be more appropriate for a variable of the RRc type, while the lightcurve in Fig. 7 is more likely that of an RRab type.

APASS J334.2845-06.0965 = FZ Aqr. This star is classified in the GCVS as a over-contact binary (W UMa type), with an orbital period of P = 0^d.6791072. The equi-potential, common-envelope surface engulfing the two components in an over-contact binary is characterized by a uniform temperature. This results in eclipses of equal depth and an absence of relevant color variation along the orbit (Duerbeck, 1996). Our data are phase plotted according to P = 0^d.6791072 in Fig. 7. While the double maxima, double minima pattern typical of over-contact binaries is seen, a large color change is present, contrary to what is expected for over-contact binaries. A period of P = 0^d.2533 produces instead a nice RRvar pulsation light-curve, with the expected color-curve, and an RRc shape appropriate for such a short period.

APASS J335.0110–08.7694 = GL Aqr. This star is reported with a dubious classification as RRvar in the GCVS, with a period P = 0^d.400193 imported from K + 06. This period is incompatible with our data, that instead provide a nice RRab light- and color-curve for P = 0^d.6640 as shown in Fig. 7. It is worth noticing that the P = 0^d.666740 listed by M + 08, even if apparently close to our period, is poorly compatible with our data.

APASS J338.7391–03.7094 = GX Aqr. Our data confirm the P = 0^d.5473216 period listed by GCVS. The dispersion of points along the light-curve, and separate branches in the color-curve suggest however the presence of a second superimposed period. We have carried out a search on the residuals from the main period, but have not been able to identify the second one.

APASS J340.3813–06.4775 = HH Aqr. Our P = 0^d.5745 and GCVS pulsation periods for this star are identical, while the period P = 0^d.36479 given by K + 06 for this star is only poorly compatible with our data.

4.3. Color-brightness correlation

There is a tight correlation between brightness and color in RRvar, bluest colors occurring near maximum brightness and reddest ones shortly before minimum. The correlation is displayed in Fig. 8, were we plot all our observations for the 53 RRvar in Table 1. The apparently broader distribution at minimum brightness is mainly due to the larger number of points there (RRvar of the RRab type spend more time at minimum than at maximum), coupled with larger observational errors at fainter magnitudes.

There are more than fifty stars within the red contoured area of Fig. 5, lying above the 4σ line in Fig. 4, that remain after the 53 RRvar with a firm period determination above described are taken out. The data for each one were overplotted on the brightness-color distribution of Fig. 8 and the results inspected. Of them, 19 stars

[2] also from www.ans-collaboration.org.

Table 1
List of discovered RR Lyr variables with a period solution on our data. The coordinates are for epoch 2012 and equinox 2000. *N* = number of observing epochs, Δ*V* = amplitude of variability recorded in the *V* band. Distances are computed according to absolute magnitude calibration by Bailey (1902), adopting the [Fe/H] = −1.0 metallicity of Aquarius stream from Wylie-de Boer et al. (2012) and reddenings from Munari et al. (2013b) galactic extinction model. Refs.: (1) GCVS, (2) Kinemuchi et al. (2006), (3) Miceli et al. (2008), (4) Hoffman and McNamara (2009).

APASS name	RA (J2000)			DEC			N	ΔV	Period (days)	Type	Mean values						*d* (kpc)	Literature			
											V	B − V	V − r′	g′ − r′	V − i′	T_{eff}(K)		Name	Type	Period	Ref
J326.1727-17.2098	21	44	41.45	−17	12	34.7	13	1.13	0.6615	ab	13.757	0.380	0.099	0.247	0.015	6455	4.09	UV Cap	RR	0.66155	2
J327.7360-16.2446	21	50	56.63	−16	14	40.4	13	0.92	0.4581	c	14.533	0.364	0.040	0.178	0.157	6725	5.78				
J327.8557-13.9697	21	51	25.38	−13	58	10.8	17	0.56	0.5781	ab	12.396	0.439	0.129	0.297	0.290	6265	2.17		RR	0.57781	2
J328.5101-14.2908	21	54	02.41	−14	17	26.4	24	1.03	0.4786	ab	14.039	0.493	0.122	0.327	0.237	6185	4.61		RR	0.47842	2
J328.5337-17.0689	21	54	08.10	−17	04	08.0	11	0.48	0.3531	c	14.915	0.308	−0.015	0.103	0.001	7030	6.92				
J328.6642-17.6785	21	54	39.38	−17	40	41.5	16	1.01	0.6127	ab	15.661	0.417	0.066	0.209	0.105	6600	9.72				
J329.4053-14.3821	21	57	37.28	−14	22	55.4	15	0.50	0.8195	ab?	13.571	0.440	0.122	0.304	0.268	6285	3.71				
J330.4745-05.4981	22	01	53.89	−05	29	53.0	11	0.49	0.2995	ab	14.038	0.288	0.004	0.094	−0.123	7150	4.63		RR	0.42822	2
J330.4809-05.6007	22	01	55.52	−05	36	02.6	15	0.73	0.5712	ab	12.060	0.360	0.047	0.159	−0.048	6840	1.85	TZ Aqr	RRab	0.571191	1
J331.0217-05.5884	22	04	05.22	−05	35	17.9	15	0.48	0.6586	ab?	14.732	0.462	0.104	0.287	0.225	6285	6.34		RR	0.658585	3
J331.1958-17.8973	22	04	47.00	−17	53	50.3	13	0.79	0.3660	ab	15.822	0.427	0.042	0.243	0.135	6575	10.47				
J331.8773-16.3343	22	07	30.60	−16	20	02.3	9	1.14	0.4805	ab	15.458	0.359	0.070	0.172	0.088	6810	8.87		RR	0.480538	3
J332.5663-16.6631	22	10	15.89	−16	39	46.8	14	0.82	0.5508	ab	13.422	0.353	0.072	0.199	0.157	6635	3.47	WX Aqr	RRab	0.5508402	1
J333.4837-14.7816	22	13	56.10	−14	46	53.6	22	0.41	0.4506	c	13.863	0.311	0.045	0.144	0.010	6950	4.25				
J333.9279-11.5018	22	15	42.63	−11	30	06.1	10	0.84	0.4979	ab?	15.364	0.331	0.042	0.129	−0.264	7025	8.47		RR	0.498026	3
J334.2845-06.0965	22	17	08.29	−06	05	47.0	13	0.41	0.2533	c	14.259	0.333	0.025	0.142	0.037	6860	5.10	FZ Aqr	WU	0.6791072	1
J334.4950-18.4028	22	17	58.80	−18	24	10.1	10	0.70	0.8897	ab	14.907	0.459	0.089	0.251	0.127	6505	6.88	AS Aqr	RRab	0.5306	1
J335.0037-18.3780	22	20	00.89	−18	22	40.9	7	0.58	0.6580	ab	15.382	0.510	0.057	0.293	0.133	6255	8.55				
J335.0110-08.7694	22	20	02.65	−08	46	09.4	14	0.86	0.6640	ab	14.748	0.475	0.116	0.308	0.175	6180	6.40	GL Aqr	RR:	0.400193	1
J335.7669-07.0001	22	23	04.00	−07	00	00.1	12	0.44	0.2937	c	14.392	0.326	0.032	0.139	0.078	6880	5.42	GO Aqr	RRc	0.2937604	1
J336.2457-10.2098	22	24	58.98	−10	12	34.7	18	1.18	0.7401	ab	14.892	0.367	0.017	0.155	−0.027	6820	6.82		RR	0.740280	3
J336.2599-04.9493	22	25	02.40	−04	56	58.2	13	1.02	0.5276	ab	13.902	0.596	0.088	0.446	−0.053	5660	4.32	FH Aqr	RRab	0.5277362	1
J336.4131-07.9412	22	25	39.19	−07	56	28.2	15	0.40	0.4052	c	10.816	0.318	0.033	0.136	0.038	6955	1.05	GP Aqr	RRc	0.405278	1
J336.4140-18.2399	22	25	39.30	−18	14	23.0	22	0.63	0.3881	c	13.404	0.285	0.028	0.110	−0.094	7085	3.43	AX Aqr	RRc	0.3881658	1
J336.9532-07.4840	22	27	48.77	−07	29	01.7	14	1.17	0.4696	ab	12.597	0.391	0.063	0.216	0.236	6600	2.38	BN Aqr	RRab	0.4696822	1
J337.1077-17.0326	22	28	25.82	−17	01	56.9	8	0.50	0.4230	ab	15.166	0.461	0.088	0.270	0.238	6390	7.76				
J337.6893-08.7295	22	30	45.49	−08	43	44.3	8	0.68	0.5721	ab	15.270	0.431	0.092	0.257	0.408	6465	8.13		RR	0.572098	3
J337.7189-07.7115	22	30	52.51	−07	42	41.1	14	1.07	0.5260	ab	13.432	0.400	0.075	0.240	0.312	6505	3.48	GW Aqr	RRab	0.5259810	1
J337.7805-12.1855	22	31	07.35	−12	11	06.6	8	0.79	0.4580	ab?	15.280	0.286	0.090	0.151	0.058	6980	8.09		RR	0.457073	3
J338.2632-11.2808	22	33	03.10	−11	16	50.4	12	0.84	0.6048	ab?	13.942	0.390	0.043	0.189	0.112	6740	4.40		RR	0.604965	3
J338.4173-08.9942	22	33	40.13	−08	59	38.5	8	0.72	0.5702	ab	15.128	0.471	0.031	0.231	0.330	6530	7.62		RR	0.569672	3
J338.7391-03.7094	22	34	57.38	−03	42	33.1	24	1.09	0.5473	ab	13.713	0.489	0.074	0.341	−0.026	6090	3.96	GX Aqr	RRab	0.5473216	1
J338.7924-14.6369	22	35	10.18	−14	38	12.6	19	0.57	0.3603	c	14.714	0.302	0.028	0.119	−0.027	7050	6.28				
J338.8881-17.9713	22	35	33.09	−17	58	16.1	13	1.11	0.4857	ab	14.178	0.326	0.061	0.202	0.037	6765	4.92	BE Aqr	RRab	0.4863896	1
J339.0161-10.0154	22	36	03.85	−10	00	55.0	16	1.14	0.6088	ab	12.885	0.367	0.045	0.165	−0.009	6915	2.72	AA Aqr	RRab	0.6088859	1
J340.0742-03.2647	22	40	17.78	−03	15	52.3	12	0.57	0.3820	c	14.632	0.317	0.031	0.158	0.104	6920	6.05				
J340.3813-06.4775	22	41	31.50	−06	28	38.8	15	0.48	0.5745	ab	12.341	0.413	0.100	0.278	0.215	6415	2.11	HH Aqr	RRab	0.5744539	1
J340.6595-15.7587	22	42	38.28	−15	45	30.8	14	0.97	0.5089	ab	13.411	0.377	0.062	0.193	0.124	6735	3.45		RR	0.50891	4
J341.6023-12.9134	22	46	24.54	−12	54	48.2	10	0.66	0.5109	ab?	13.086	0.301	0.007	0.074	−0.350	7210	2.98		RR	0.51099	4
J342.3612-01.9490	22	49	26.69	−01	56	56.5	16	0.62	0.5760	ab	14.143	0.552	0.074	0.356	0.204	6065	4.83				
J342.9223-12.6093	22	51	41.35	−12	36	33.4	12	0.51	0.3771	ab	13.984	0.295	0.024	0.118	0.040	7040	4.53				
J343.4722-06.1203	22	53	53.32	−06	07	12.6	8	0.97	0.6567	ab?	15.509	0.398	0.119	0.268	0.049	6525	9.08		RR	0.656095	3
J343.5345-12.3607	22	54	08.27	−12	21	38.1	14	0.90	0.6940	ab	12.095	0.368	0.064	0.195	0.131	6745	1.89	BO Aqr	RRab	0.6940301	1
J343.8897-06.0984	22	55	33.51	−06	05	53.1	7	1.01	0.5072	ab?	15.039	0.363	0.056	0.223	0.078	6665	7.31		RR	0.507577	3
J344.4040-07.3089	22	57	36.96	−07	18	32.0	9	0.61	0.4318	c?	15.665	0.454	0.100	0.243	−0.053	6580	9.77				
J344.6874-06.3547	22	58	44.97	−06	21	16.7	8	0.41	0.3585	c	14.685	0.411	−0.002	0.167	−0.243	6770	6.22				
J345.1054-08.8553	23	00	25.30	−08	51	18.3	14	0.52	0.4405	c	14.216	0.320	0.034	0.132	0.029	7025	5.01				
J345.2350-09.6496	23	00	56.44	−09	38	57.1	11	0.97	0.5462	ab	14.980	0.356	0.062	0.173	−0.010	6845	7.11	BP Aqr	S:		1
J345.5465-06.8863	23	02	11.15	−06	53	09.3	7	0.67	0.3230	c	15.586	0.497	0.095	0.323	−0.008	6145	9.42				
J349.9028-06.7960	23	19	36.68	−06	47	45.7	11	1.20	0.5491	ab	14.841	0.365	0.117	0.219	−0.007	6690	6.64				
J351.0548-12.6323	23	24	13.18	−12	37	56.1	13	1.11	0.5187	ab	13.102	0.382	0.056	0.230	0.129	6580	2.99	HQ Aqr	RRab	0.5188923	1
J351.8289-12.6475	23	27	18.94	−12	38	50.8	13	0.57	0.5252	c	13.903	0.376	0.074	0.238	0.074	6590	4.32				
J353.9485-10.9905	23	35	47.60	−10	59	25.5	12	0.88	0.5525	ab	14.038	0.406	0.068	0.232	0.155	6675	4.61	HR Aqr	RRab	0.552666	1

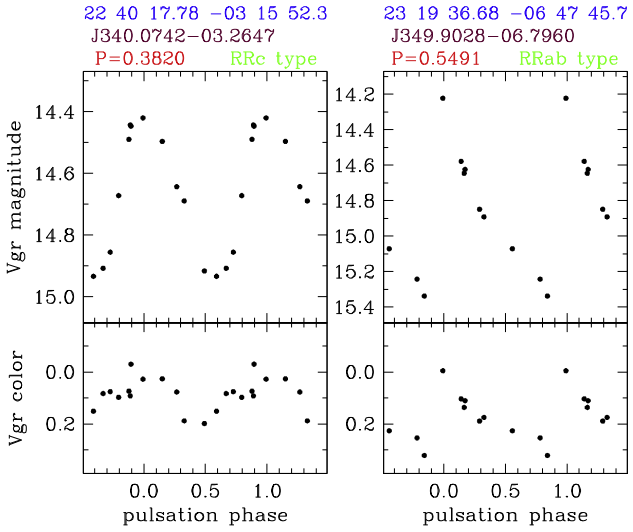

Fig. 6. The light- and color-curves of two newly discovered RR Lyr variables. They have been selected to illustrate the typical sinusoidal shape of light- and color-curves for RR Lyr variables of the RRc type, and the triangular-like shape of RRab type. They are also an example of the light- and color-curves provided in Figs. S14–S18 (available electronic only) for all the 53 RR Lyr variables discovered in our survey for which we were able to derive the pulsation period (Table 1). For the definition of *Vrg* magnitudes and colors see Eqs. (1) and (2).

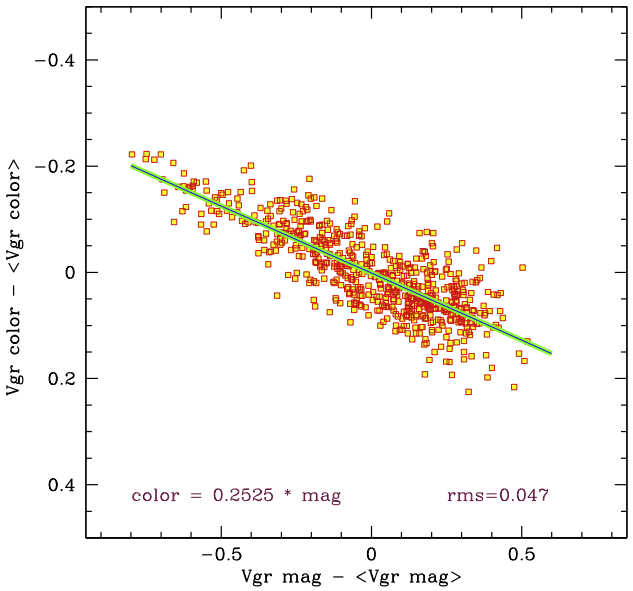

Fig. 8. The tight correlation exhibited by the discovered RR Lyr variables in the *Vgr* brightness – color plane (*Vgr* magnitude and *Vgr* color as defined in Eqs. 1 and 2).

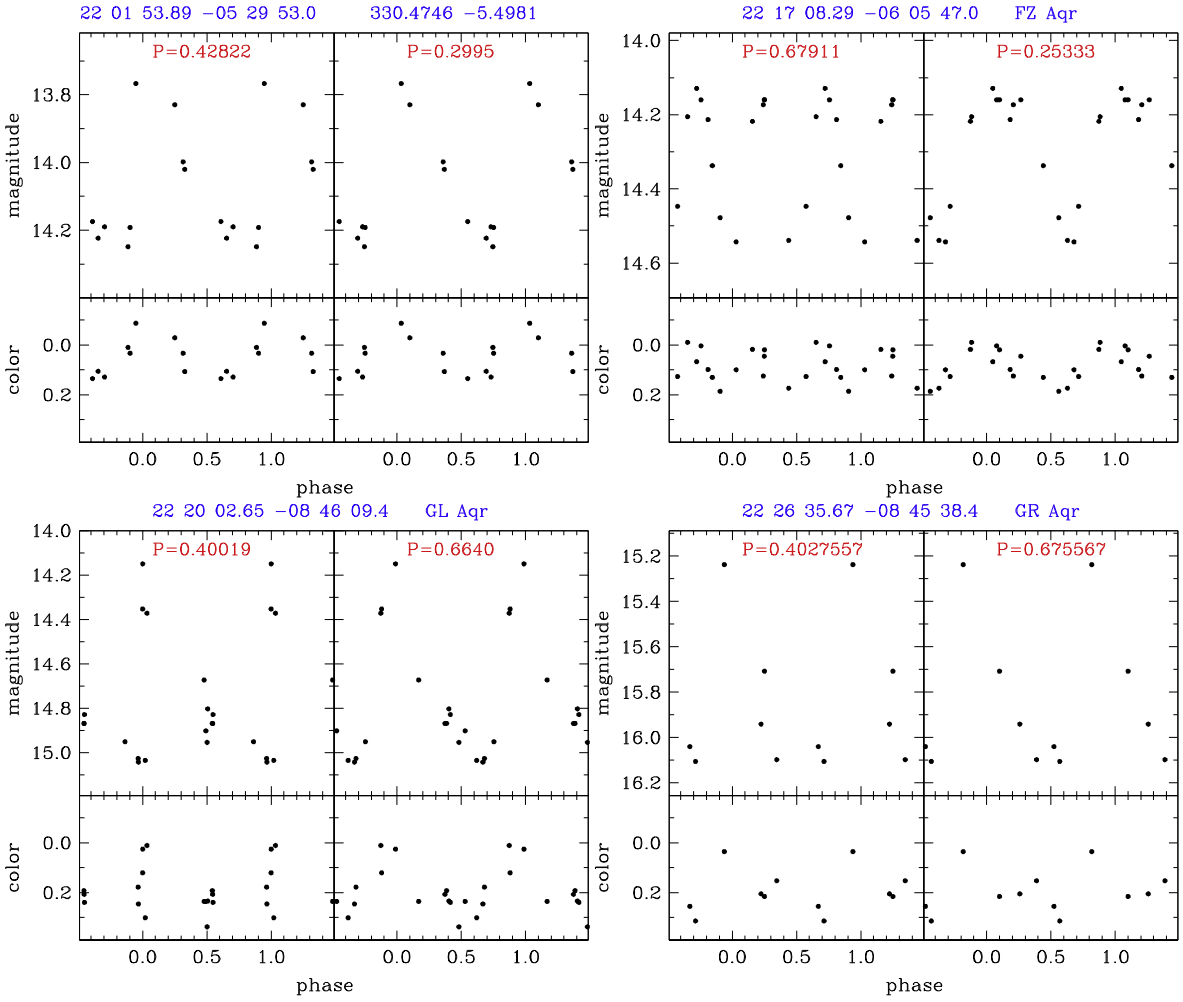

Fig. 7. Light- and color-curves of a few individual objects discussed in Sections 4.2 and 4.3.

showed a brightness-color distribution closely matching that of Fig. 8, and were considered as bona fide RRvar themselves even if our data were not able to derive their pulsation period (mainly because of the small number of available observing epochs, just 5 on the median). They are listed in Table 2. After compiling Table 2 we turned to the literature, and it was reassuring to find that eight of them were already known as RRvar, boosting the confidence in a true RRvar nature for the remaining eleven. There is one star worth noting individually.

APASS J336.6488–08.7611 = GR Aqr. The pulsation period assigned to this star by M + 08 is P = 0^d.675567, while the GCVS lists P = 0^d.4027557. The GCVS period provides good looking light- and color-curves when plotted against our data, while the M + 08 one performs somewhat better (cf. Fig. 7).

4.4. Fainter RR Lyr variables

There are 45 additional stars classified in literature as RRvar that lie within the surveyed area of Fig. 1. They are listed in Table 3. Nearly all of them are much fainter than the completness limit of our survey: 29 of these 45 RRvar have been detected at least once by our observations (their average magnitude on our observations is $V = 16.50$), while the remaining 16 RRvar were never detected (their average magnitude from literature data is $V = 17.90$). Our data are enough in number and accuracy to confirm the variability of 10 of these 45 stars. The three brightest of them (see details below), for which we have the largest amount of observations, do not look like genuine RRvar, casting doubts on a real RRvar nature for the other entries listed in Table 3.

APASS J337.9847-12.3557. This star is listed by M + 08 as a RRvar of period P = 0^d.628342 and amplitude $\Delta V = 0.352$. When our accurate 14 measurements for this star are plotted against this period, they distribute randomly and with a lower $\Delta V = 0.157$ amplitude. Furthermore, the APASS data does not fit the brightness-color correlation for RRvar of Fig. 8. Thus, while this star is probably variable, it does not look like a RRvar.

APASS J339.7217-06.5402. This star is listed by M + 08 as a RRvar of period P = 0^d.732023 and amplitude ΔV=0.419. Both these values are moderately compatible with available APASS observations, however our data does not fit the brightness-color correlation for RRvar of Fig. 8.

APASS J343.3673-10.4766. This star is listed by M + 08 as a RRvar of period P = 0^d.595970 and amplitude ΔV=0.478. The APASS data plotted against this period does not return the light- and color-curve expected from an RRvar.

4.5. White-light to V band magnitude trasformation

The distance to a RRvar is obviously related to its mean apparent magnitude, and the calibration of the absolute magnitude is available only for well defined photometric bands. K + 06 and M + 08 have transformed the mean white-light magnitude of RRvar discovered by ROTSE-I and LONEOS surveys into V-band equivalents. In Fig. 9 we compare our mean magnitude obtained directly in the V-band with the corresponding K + 06 and M + 08 values for the stars in common. In both cases the rms is compatible with the effect of the limited amount of points used to define the lightcurves and therefore their mean value, and the long term modulation (Blazhko effect) that about 1/3 of known RRvar display. For both K + 06 and M + 08 there seems to be present both a limited color dependence and a modest offset.

4.6. Photometric sequences for follow-up observations

The light- and color-curves of RRvar presented in this paper are composed of a limited number of points. Appreciation of finer

Table 2
List of discovered RR Lyr variables without a firm period solution on our data. The coordinates are for epoch 2012 and equinox 2000. N = number of observing epochs, ΔV = amplitude of variability recorded in the V band. Distances are computed according to absolute magnitude calibration by Bailey, 1902, adopting the [Fe/H] = −1.0 metallicity of Aquarius stream from Wylie-de Boer et al., 2012 and reddening from Munari et al., 2013b galactic extinction model. Refs.: (1) GCVS, (2) Kinemuchi et al. (2006), (3) Miceli et al. (2008).

APASS name	RA (J2000)	DEC	N	ΔV	Period (days)	Mean values					T_{eff} (K)	d (kpc)	Literature			
						V	B − V	V − r′	g′ − r′	V − i′			Name	Type	Period	Ref
J326.9389-14.1113	21 47 45.32	−14 06 38.9	7	0.597		15.843	0.247	0.136	0.142	0.357	6900	10.58				
J330.2537-14.9661	22 01 00.88	−14 57 57.9	10	0.564		15.149	0.341	0.056	0.176	0.080	6795	7.69				
J332.5445-14.9057	22 10 10.74	−14 54 19.6	7	0.953		15.576	0.388	0.040	0.108	−0.114	7200	9.36		RR	0.620975	3
J336.0969-15.6349	22 24 23.25	−15 38 05.5	14	0.487		14.371	0.279	0.008	0.132	−0.095	6990	5.37				
J336.6488-08.7611	22 26 35.67	−08 45 38.4	8	0.938		15.794	0.371	0.071	0.272	0.251	6265	10.34	GR Aqr	RRab	0.4027557	1
J336.9290-10.1514	22 27 42.99	−10 09 04.1	6	0.488		15.925	0.487	0.092	0.291	−0.106	6360	10.99		RR	0.624097	3
J336.9453-04.7179	22 27 46.92	−04 43 03.3	6	0.820		15.544	0.647	−0.062	0.356	0.376	6015	9.22				
J337.5724-20.1630	22 30 17.38	−20 09 46.8	8	0.532	0.67133?	15.536	0.406	0.129	0.263	0.222	6485	9.19				
J338.2706-16.9331	22 33 04.94	−16 55 59.2	6	1.108		15.441	0.327	0.038	0.185	−0.015	7175	8.79				
J338.3748-13.5594	22 33 29.93	−13 33 33.2	7	0.839		15.134	0.433	0.023	0.214	0.049	6645	7.63				
J338.7505-09.6799	22 35 00.14	−09 40 47.5	9	0.824	0.59307?	15.677	0.455	−0.028	0.175	0.145	6700	12.09		RR	0.592958	3
J339.0801-17.3155	22 36 19.20	−17 18 55.2	6	0.840		13.995	0.398	0.056	0.203	−0.172	6830	4.52		RR	0.53309	2
J343.3673-10.4766	22 53 28.16	−10 28 35.8	7	0.401		15.316	0.404	0.078	0.227	0.326	6530	8.30		RR	0.595970	3
J343.4390-02.8159	22 53 45.36	−02 48 57.0	15	0.719		14.025	0.452	0.120	0.286	0.246	6330	4.58				
J349.3524-10.5479	23 17 24.58	−10 32 52.3	7	0.597		15.100	0.488	0.027	0.266	0.066	6410	7.51				
J350.7492-08.2429	23 22 59.81	−08 14 34.4	3	0.856		15.974	0.455	0.097	0.161	0.335	6400	11.24				
J352.0914-06.7590	23 28 21.93	−06 45 32.4	5	0.735		15.776	0.451	0.083	0.289	9.999	6140	10.26				
J354.6373-09.3190	23 38 32.89	−09 19 07.5	8	0.686	0.48?	11.753	0.211	0.045	0.082	0.023	7485	1.46	BR Aqr	RRab	0.4818713	1

Table 3
List of all remaining RR Lyr variables from literature that are not included in Tables 1 and 2 and are present within the boundaries of the surveyed field in Fig. 1. Nearly all of them are much fainter than the completeness limit of our survey ($V = 15.2$) or its faint limit ($V = 16.2$). N = number of our observations. Last column gives comments on the object nature based on our data. Identifiers: [KMP2008] Keller et al., 2008, [MRS2008] Miceli et al., 2008, FASTT Henden and Stone, 1998, [SIG2010] Sesar et al., 2010, NSVS Hoffman and McNamara, 2009. Distances computed according to absolute magnitude calibration by Bailey, 1902, adopting the [Fe/H]=−1.0 metallicity of Aquarius stream from Wylie-de Boer et al. (2012) and reddening from Munari et al. (2013b) galactic extinction model.

Literature		d	APASS	RA (J2000) DEC		N	Notes
Name	V	(kpc)	Name				
[KMP2008]115381.349	16.80	16.44	J326.2729-15.6737	21 45 05.41	−15 40 27.4	1	
[MRS2008]327.500275-15.452437	16.38	13.55	J327.5009-15.4521	21 50 00.04	−15 27 08.8	1	
[MRS2008]327.561279-17.063532	16.51	14.38	J327.5613-17.0633	21 50 14.71	−17 03 48.7	2	var
[MRS2008]327.892181-16.038532	16.53	14.52	J327.8927-16.0387	21 51 34.09	−16 02 18.6	3	
[MRS2008]328.220032-15.780692	16.63	15.20	J328.2202-15.7806	21 52 52.81	−15 46 50.5	2	
[MRS2008]329.458252-14.605897	16.38	13.55	J329.4581-14.6059	21 57 49.98	−14 36 21.2	3	
[MRS2008]330.291351-17.158651	16.34	13.30	J330.2913-17.1588	22 01 09.92	−17 09 31.1	2	var
[MRS2008]331.352386-13.587284	17.04	18.36	J331.3523-13.5869	22 05 24.58	−13 35 14.4	1	
[MRS2008]332.210693-03.712178	15.90	10.86	J332.2112-03.7108	22 08 50.57	−03 42 43.8	1	
[MRS2008]332.220734-13.326912	16.94	17.53	J332.2208-13.3268	22 08 52.98	−13 19 36.9	2	
[MRS2008]332.471252-03.690646	16.72	15.84	J332.4711-03.6907	22 09 53.10	−03 41 26.3	2	var
[MRS2008]333.047119-16.579510	16.27	12.88	J333.0472-16.5794	22 12 11.31	−16 34 46.2	4	var
[MRS2008]333.917664-18.633589	16.89	17.13	J333.9176-18.6336	22 15 40.21	−18 38 01.1	1	
[MRS2008]334.499725-19.017044	16.63	15.20	J334.4997-19.0177	22 17 59.93	−19 01 01.4	2	var
[MRS2008]335.067780-08.236611	16.33	13.24	J335.0675-08.2365	22 20 16.27	−08 14 11.8	2	
[MRS2008]335.113220-10.757199	16.38	13.55	J335.1132-10.7572	22 20 27.17	−10 45 25.9	2	
[MRS2008]335.147919-15.793706	17.07	18.62	J335.1475-15.7940	22 20 35.50	−15 47 37.3	1	
[MRS2008]335.658508-10.159719	16.20	12.47	J335.6587-10.1601	22 22 38.04	−10 09 35.0	4	var
[MRS2008]337.984528-12.355494	13.65	3.85	J337.9847-12.3557	22 31 56.29	−12 21 19.8	14	var, not RR type
[MRS2008]338.677582-10.795616	17.05	18.45	J338.6771-10.7959	22 34 42.62	−10 47 44.2	2	
[MRS2008]338.967377-05.294749	17.31	20.79	J338.9676-05.2951	22 35 52.17	−05 17 41.1	1	
[MRS2008]339.721527-06.539852	15.55	9.24	J339.7217-06.5402	22 38 53.18	−06 32 23.4	5	var, not RR type
FASTT 1587	16.64	15.27	J340.5648-00.6742	22 42 15.62	−00 40 26.9	2	
[SIG2010]719834	16.66	15.41	J340.7504-01.2324	22 43 00.10	−01 13 56.6	1	
[MRS2008]341.856964-05.523699	16.48	14.19	J341.8568-05.5234	22 47 25.70	−05 31 25.7	4	
[SIG2010]848438	16.37	13.49	J342.6779-00.1289	22 50 42.71	−00 07 43.9	1	
[MRS2008]343.085663-06.991775	16.39	13.61	J343.0854-06.9918	22 52 20.56	−06 59 30.4	1	
[MRS2008]343.367126-10.476358	15.14	7.65	J343.3673-10.4766	22 53 28.11	−10 28 34.9	7	var, not RR type
NSVS 1740775	14.17	4.90	J350.8918-08.0125	23 23 34.02	−08 00 44.9	4	var
below APASS detection threshold							
[MRS2008]328.475128-16.104023	17.38	21.47					
[MRS2008]329.213043-16.723717	17.11	18.96					
[MRS2008]331.601410-03.799698	16.97	17.78					
[MRS2008]334.018066-15.500797	17.42	21.87					
[MRS2008]336.533112-06.848556	16.83	16.67					
[MRS2008]337.386078-05.003536	17.01	18.11					
[MRS2008]337.874298-07.474282	17.44	22.07					
[MRS2008]340.769989-06.973113	17.29	20.60					
FASTT 1594	16.91	17.29					
[SIG2010]744810	18.39	34.19					
[SIG2010]785754	19.78	64.85					
[SIG2010]834891	17.57	23.44					
[SIG2010]837937	20.01	72.09					
[SIG2010]765345	17.25	20.22					
[SIG2010]873466	18.36	33.72					
[SIG2010]778130	19.25	50.80					

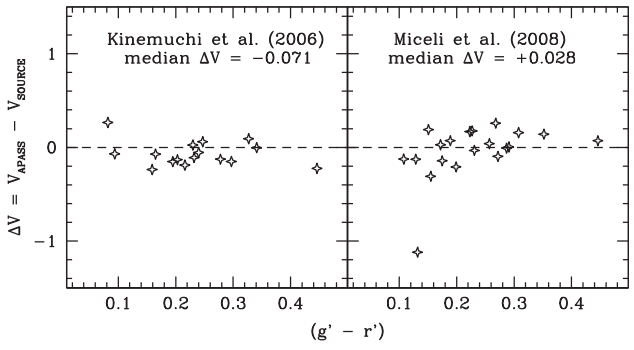

Fig. 9. Comparison between our mean V magnitudes and those derived by Kinemuchi et al. (2006) and Miceli et al. (2008) from their white-light observations for the RR Lyr in common with us.

details of the light-curves and refinements of the derived pulsation periods would benefit from additional observations. Towards this aim, to facilitate the work of follow-up observers, we have derived accurate photometric comparison sequences around all the RRvar discussed in this paper. They are tabulated in Table 4 and plotted in Figs. S19–S22 (both available in their entirety in electronic form only[3]). The median number of independent epochs of measurements for the photometric sequences is 14, and the median errors of the magnitudes is 0.009 mag for B, 0.007 mag for V, 0.007 mag for g, 0.006 mag for r, and 0.023 mag for i. Magnitudes for the stars in the photometric comparison sequences are tabulated also for the Landolt R_C and I_C bands, derived from APASS Landolt V and Sloan g, r, i following the transformations (see Henden (2013) for a detailed discussion):

[3] also from www.ans-collaboration.org.

Table 4
Photometric sequences around the discovered RR Lyr variable stars (the table is published in its entirety in the electronic edition of the journal. A small portion is shown here for guidance regarding its form and content). The stars are identified in the finding chart of Fig. 10.

	RA	DEC	B (±err)		V (±err)		g'(±err)		r'(±err)		i'(±err)		R_c	I_c	Number of epochs				
															B	V	g'	r'	i'
APASS J336.413138-07.941218 22 25 39.2 −07 56 28.4																			
A	336.293630	−8.030791	12.722	0.005	12.390	0.004	12.499	0.004	12.382	0.008	12.481	0.024	12.216	12.115	17	17	17	17	20
B	336.341122	−7.908038	13.735	0.009	13.045	0.005	13.343	0.007	12.840	0.003	12.698	0.011	12.639	12.287	15	15	15	15	15
C	336.344271	−7.926141	13.861	0.011	13.196	0.003	13.486	0.006	13.045	0.005	12.952	0.016	12.851	12.549	14	14	15	15	14
D	336.476066	−8.051349	14.293	0.007	13.643	0.005	13.929	0.004	13.458	0.005	13.283	0.011	13.257	12.872	13	13	13	13	13
E	336.477500	−8.086694	13.664	0.002	12.957	0.005	13.272	0.003	12.766	0.005	12.580	0.014	12.562	12.166	14	14	14	14	14
F	336.493900	−7.887896	12.838	0.009	11.905	0.005	12.329	0.008	11.624	0.006	11.337	0.015	11.399	10.902	15	15	15	15	15
G	336.556928	−7.977084	13.439	0.005	12.711	0.003	13.031	0.003	12.515	0.004	12.336	0.024	12.311	11.922	14	14	14	14	15
H	336.575772	−7.977360	13.174	0.004	12.606	0.003	12.850	0.003	12.481	0.002	12.340	0.010	12.288	11.939	14	14	14	14	14

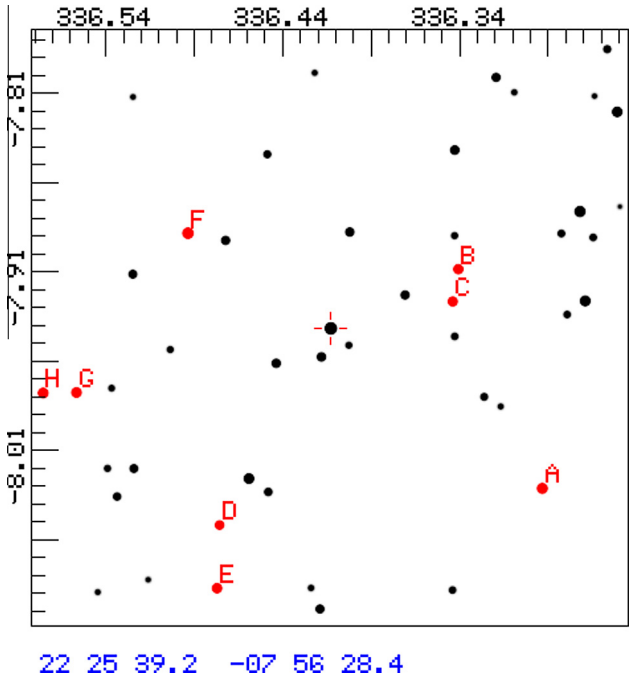

Fig. 10. Example of one of the finding charts provided in electronic form for all discovered RR Lyr variables (Figs. S19–S22). The stars forming the photometric comparison sequence (cf. Table 4) are highlighted in red and labelled with a letter. The RR Lyr variable is at the center, marked by the cross, the field is 20 × 20 arcmin and the orientation is North at the top, East to the left. (For interpretation of the references to colour in this figure caption, the reader is referred to the web version of this article.)

$$I_C = i' - 0.3645 - 0.0743 \times (g - i) + 0.0037 \times (g' - i')^2 \quad (3)$$

$$R_C = r' - 0.1712 - 0.0775 \times (V - i') = -0.0290 \times (V - i')^2 \quad (4)$$

The sequences are contained within a square area of 20 × 20 arcmin centered on the variable, and are composed of at least 8 stars safely away from the saturation limits. Within the sparsely populated field, we have selected the (obviously non variable) comparison stars that best satisfy the following criteria: (i) typically 1 mag brighter than the variable, and (ii) a color range that extends for $\Delta(B - V) \geqslant 0.5$ mag and covers (or is the closest possible choice to) the range of colors displayed by the variable (see Fig. 10).

4.7. Spatial distribution

The distribution on the sky of the 71 discovered RRvar is presented in Fig. 11. It appears homogeneous within the statistical

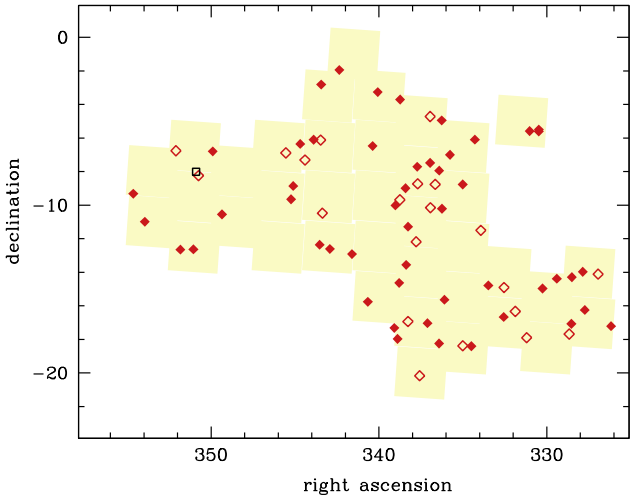

Fig. 11. Distribution on the plane of the sky of the 71 validated RR Lyr variables (Tables 1 and 2). Solid diamonds: stars within 8 kpc. Open diamonds: stars between 8 and 11 kpc.

fluctuations. This could either indicate a similar efficiency detection everywhere over the explored area of the sky or the absence of marked spatial grouping by AqS. The latter in turn would signify that AqS RRvar members are spread uniformly over the whole area (similarly to the non-variable known members) and/or that they are appreciably less in number than the unrelated field RRvar.

4.8. Period–amplitude distribution

The period–amplitude distribution (V band) for the 53 RRvar of Table 1 is shown in Fig. 12 (upper left panel), where it is compared with the equivalent distributions for all the RRvar listed in the GCVS and all those discovered by K + 06, M + 08 and H + 09 among the stars detected in the course of ROTSE-1 and LONEOS surveys mentioned above.

The 2013 on-line version of GCVS lists a total of 8241 RRvar, 596 of the RRc type, 5142 of the RRab type, and the remaining 2503 of uncertain or unassigned type. The proportion is RRab/RRc = 8.6. In our data it is RRab/RRc ∼ 2.5. This is related to the so-called *Oosterhoff dichotomy* (Oosterhoff, 1939; Kolenberg, 2012). Globular clusters of the Oosterhoff type I (such as M3 and M5) are metal richer and have RRab/RRc≫1, while Oosterhoff type II clusters (like M15 and M53) are metal poorer and for them RRab/RRc ∼ 1. The mean pulsation periods of both the RRab and RRc varieties is shorter in Oosterhoff type I clusters, 0.55 and 0.32 days respectively, than in type II clusters, 0.64 and 0.37 days respectively (Kolenberg,

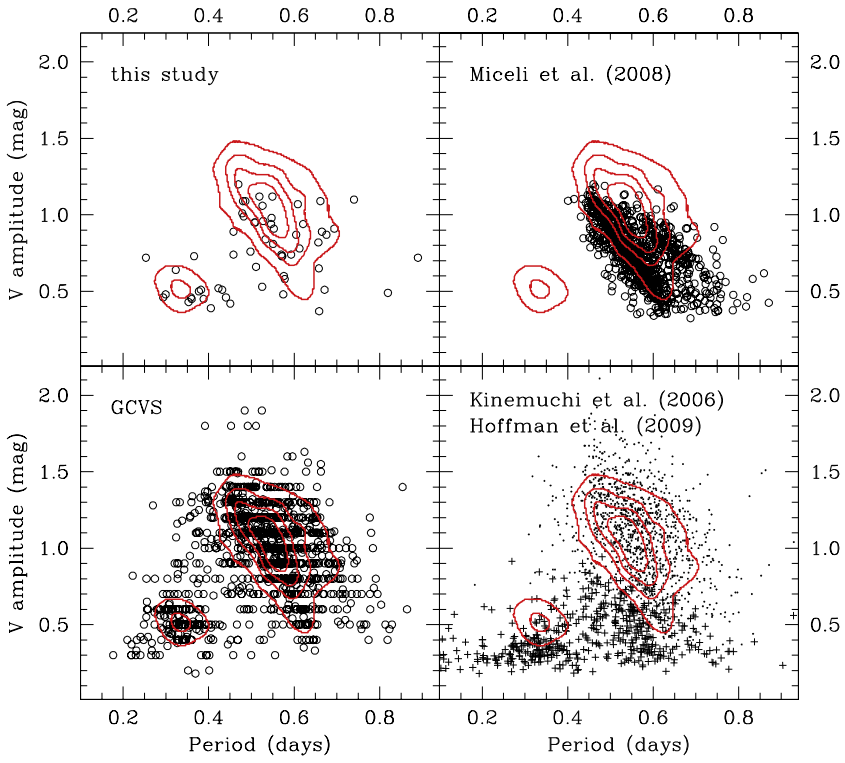

Fig. 12. Period versus *V*-band amplitude relation for the RR Lyr variables in this study and from literature. GCVS: General Catalog Variable Stars (2013 on-line edition). The GCVS data show a discrete distribution in ordinates because maximum and minimum brightness (from which amplitude is computed) is only given to a single digit for a large number of objects. Kinemuchi et al. (2006) data are plotted as dots, Hoffman and McNamara (2009) data as crosses. Isocontours are drawn at 20%, 40%, 60% and 80% of peak density for GCVS distribution, and are repeated in the other panels for reference. The concentration of points at shorter periods and lower amplitudes marks the locus of RRc type variables (pulsating in the first overtone mode), while the large concentration at twice the period and amplitude is populated by the RRab type (fundamental mode pulsators).

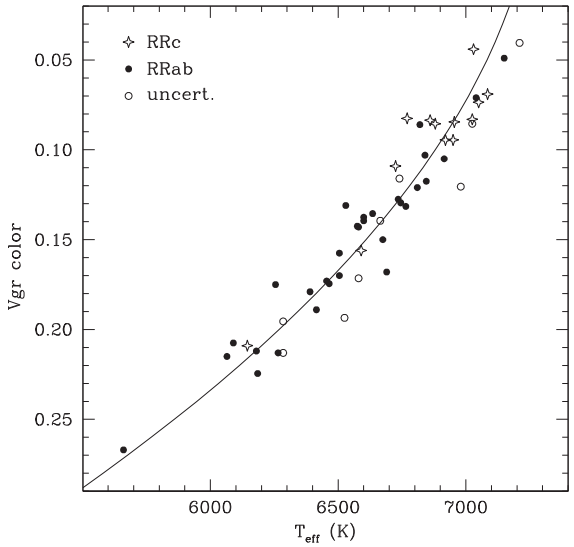

Fig. 13. Relation between *Vgr* color (defined in Eq. 2) and $T_{\rm eff}$ for the stars in Table 1. The 2nd order polynomial fit is given in Eq. (7).

2012). The RRab/RRc ratio and the mean pulsation periods of the RRab and RRc variables we discovered suggest a mix of possible origins for them. The higher proportion of RRc type variables that we found with respect to GCVS may be also related to the high accuracy of our period search and lightcurve analysis, supported by detailed color information which is generaly missing in other surveys, and is surely missing for a large body of historical observations of RRvar listed in the GCVS (in particular those historically discovered on blue-sensitive patrol plates). RRc types are notoriously difficult to discover for two main reasons: their amplitudes are appreciably lower than RRab types (cf. Fig. 12) and their nearly sinusoidal light-curves (cf. Fig. 6) often confuse them with over-contact binaries, which are quite abundant among field stars (cf. the above discussion on APASS J334.2845-06.0965 = FZ Aqr).

M + 08 did not look for RRc variables in the LONEOS data, and therefore this type of variable is missing in their data plotted in Fig. 12. The distribution in Fig. 12 of RRvar from ROTSE-I is different among the two principal investigations, K + 06 and H + 09, reflecting different discovery approaches. ROTSE-I RRvar populate a broader fraction of the plane, suggesting lower accuracy in the results. In particular, the distribution of H + 09 data is far away from the other data, suggesting either (i) a large underestimate of the amplitude of variation (a factor of 2× or larger), or (ii) a heavy contamination by erronously classified RRvar, like δ Sct variables and/or over-contact binaries (W UMa type).

4.9. Colors and effective temperatures

To extract an estimate of the temperature of the RRvar discovered in this paper, we performed a χ^2 fit of the average values of photometry listed in Tables 1 and 2 against a library of purposefully-built synthetic photometry. The source stellar energy distributions are the atmospheric flux models of Castelli and Kurucz (2003). Their model atmospheres are the basis of the Munari et al. (2005) synthetic spectral atlas, which has been used to derive atmospheric parameters from spectra in recent RAVE Data Releases (Zwitter et al., 2008; Siebert et al., 2011). The atmospheric flux models of Castelli and Kurucz (2003) cover, at regular steps, a wide portion of the atmospheric parameter space in effective temperature

($T_{\rm eff}$), surface gravity ($\log g$), and metallicity ([Fe/H]). Two values of the enhancement in α-elements ([α/Fe]) are considered (0.0 and + 0.4), while the micro-turbulence is constant at 2 km sec^{-1}.

The magnitudes in the five bands of interest (B, V, g, r, i) were obtained on all input atmospheric flux models by direct integration:

$$\mathrm{mag} = -2.5 \log \frac{\int 10^{(-0.4 R_\lambda E_{B-V})} I(\lambda) S(\lambda) d\lambda}{\int S(\lambda) d\lambda} + \mathrm{const} \quad (5)$$

where I (λ) is the flux distribution of the atmospheric model, and S (λ) is the transmission profile of the given photometric band. The zero-points were set to match the observed values for the primary photometric standard of the Sloan system BD + 17.4708, for which there are several published determinations of the atmospheric parameters. The corresponding mean values are $T_{\rm eff}$ = 5980, $\log g$ = 3.85 and [M/H] = −1.72. An α-enhanced atmospheric flux model for these parameters was obtained by parabolic interpolation from Castelli and Kurucz (2003), and it was reddened by E_{B-V} = 0.010 following Ramírez et al (2006). The zero points in Eq. (2) then follow from the requirement that the computed values match the observed B = 9.911, V = 9.467, g = 9.640, r = 9.350, i = 9.250 (from Fukugita et al., 1996 and Smith et al., 2002).

To derive the effective temperature, the observed B, V, g, r, i magnitudes (mag*) were first dereddened and then χ^2 fitted to the synthetic photometric grid:

$$\chi^2 = \sum_i \frac{(\mathrm{mag}_i^* - \mathrm{mag}_i)^2}{\epsilon_i^2} \quad (6)$$

where i sums over the five photometric bands and ϵ_i are the errors of the mean values quoted in Tables 1 and 2. Given the very low reddening encountered at the high galactic latitude of Aquarius (E_{B-V}∼0.05), to deredden the observed photometric data of Tables 1 and 2 we assume a simple model for the distribution of dust in the solar suburbs in agreement with average values in literature (cf Munari et al., 2013b): a homogeneous slab of dust, extending symmetrically for 140 parsecs above and below the Galactic plane, causing a total reddening E^{pole}_{B-V} = 0.036 at the Galactic poles, with the Sun positioned on the Galactic plane. The χ^2 fit was limited to a subset of the synthetic photometric grid, defined by [α/Fe] = +0.4, $-0.75 \geqslant$ [Fe/H] $\geqslant -1.25$, and $2 \leqslant \log g \leqslant 3$, to reflect the mean properties expected for RRvar belonging to AqS and also for RRvar in general. The resulting $T_{\rm eff}$ are listed in Tables 1 and 2, and the relation between the temperature so derived and the *Vgr* color as defined in Eq. (2) is illustrated in Fig. 13, where the second order polynomial fit overplotted to the data is given by

$$T_{\rm eff}(\mathrm{K}) = 7215 - 1960 * (Vgr\ \mathrm{color}) - 13856 * (Vgr\ \mathrm{color})^2 \quad (7)$$

The distribution of observed points along this curve is characterized by an r.m.s. = 92 K. In Fig. 13, the RRc stars are grouped toward the bluest colors and hotter temperatures, as normally found in HR diagrams of globular clusters, while RRab stars are more widely distributed and shifted toward redder colors and cooler temperatures.

5. Conclusions

The aim of this paper (cf setc. 2) was to provide a nearly complete as possible census of all RRvar within a distance of 8 kpc from the Sun in the direction of the known members of the Aquarius stream discovered by W + 11 and characterized by W + 12. This translates into detecting all RRvar brighter than $V \sim 15$ mag. We are confident that we have met the goal because (1) we have been able to independently re-discover *all previously known* RRvar brighter than this limit, and (2) the distribution in magnitude of the RRvar we discover is identical with that of the field stars, which looks complete up to V = 15.2 mag (cf Fig. 3). The lists in Table 1 and 2 can now be used as inputs for follow-up high resolution spectroscopic observations, aiming to segregate RRvar members of the Aquarius stream from those belonging to the field, by deriving their barycentric radial velocities and their metallicity and comparing them with the values found by W + 12 for the Aquarius stream.

Acknowledgements

We would like to thank Ken Freeman (ANU, Camberra, Australia) for valuable discussions and support on this project. APASS is funded through a grant from the Robert Martin Ayers Sciences Fund. This research has made use of the SIMBAD database, operated at CDS, Strasbourg, France.

Appendix A. Supplementary data

Supplementary data associated with this article can be found, in the online version, at http://dx.doi.org/10.1016/j.newast.2013.07.007.

References

Bailey, S.I., 1902. Ann. Har. Coll. Obs 38, 1.
Benedict, G.F. et al., 2011. AJ 142, 187.
Castelli, F., Kurucz, R.L., 2003. IAUS 210, 20P.
Duerbeck, H.W., 1996. In: Sterken, C., Jaschek, C. (Eds.), Light Curves of Variable Stars. CUP Publishing, p. 183.
Fukugita, M., Ichikawa, T., Gunn, J.E., Doi, M., Shimasaku, K., Schneider, D.P., 1996. AJ 111, 1748.
Henden, A.A., Stone, R.C., 1998. AJ 115, 296.
Henden A.A., et al. 2013. AJ, submitted for publication.
Hoffman, D.I., Harrison, T.E., McNamara, B.J., 2009. AJ 138, 466.
Keller, S.C., Murphy, S., Prior, S., Da Costa, G., Schmidt, B., 2008. ApJ 678, 851.
Kinemuchi, K., Smith, H.A., Woźniak, P.R., McKay, T.A.ROTSE Collaboration, 2006. AJ 132, 1202.
Kolenberg, K., 2012. JAVSO 40, 481.
Landolt, A.Ü., 2009. AJ 137, 4186.
Miceli, A. et al., 2008. ApJ 678, 865.
Munari, U., Sordo, R., Castelli, F., Zwitter, T., 2005. A&A 442, 1127.
Munari, U. et al., 2012. BaltA 21, 13.
Munari U., et al. 2013a. JAD, submitted for publication.
Munari U., et al. 2013b. A&A, submitted for publication.
Munari, U., Moretti, S., 2012. BaltA 21, 22.
Oosterhoff, P.T., 1939. Observatory 62, 104.
Ramírez, I., Allende Prieto, C., Redfield, S., Lambert, D.L., 2006. A&A 459, 613.
Sesar, B. et al., 2010. ApJ 708, 717.
Shapley, H., 1918. ApJ 48, 89.
Siebert, A. et al., 2011. MNRAS 412, 2026.
Smith, J.Ã. et al., 2002. AJ 123, 2121.
Smith, H.A., 2012. JAVSO 40, 327.
Steinmetz, M. et al., 2006. AJ 132, 1645.
Williams, M.E.K. et al., 2011. ApJ 728, 102.
Wylie-de Boer, E., Freeman, K., Williams, M., Steinmetz, M., Munari, U., Keller, S., 2012. ApJ 755, 35.
Zwitter, T. et al., 2008. AJ 136, 421.